Design Considerations of a Six Phase PM-Assisted Synchronous Reluctance Machine With 4-Pole-12-Pole Configuration for Efficient Extended Speed Range Operation in Electric Vehicles

Veena Prasanna, *Student Member, IEEE*, Kunal Layek, *Member, IEEE*, and Kamalesh Hatua, *Member, IEEE*

***Abstract*—In this article, the detailed analysis of a multipole permanent magnet-assisted synchronous reluctance machine is presented which can cater to the needs of EV applications. The rotor of the machine has a 4-pole (n-pole) synchronous reluctance machine (SynRM) structure, and a 12-pole ($3n$-pole) permanent magnet (PM) structure. There exist two rotating magnetic fields in the air gap of the machine with poles in the ratio of 1:3. A single stator houses two sets of 3-ϕ windings, corresponding to each pole. To ensure steady torque operation, the supply frequencies are also kept in the ratio of 1:3. While designing, base speed of the SynRM is kept at a lower speed (say N), and that of PM is kept at the maximum speed (say N_{max}). Both components are operated till an intermediate speed, after which, the excitation of SynRM is removed without the use of any switches, since the back-EMF in SynRM due to PM is negligible. Only the PM part is operated till maximum speed, without entering field-weakening (FW). Hence, the proposed machine can be used to obtain extended speed with improved efficiency due to the absence of extra FW current. The proposed concepts are used to design a 1-kW 4 pole-12pole PMaSynRM. The designed machine is manufactured and tested in a closed loop for experimentation and validation.**

***Index Terms*—Multipole, permanent magnet-assisted synchronous reluctance machine, permanent magnet (PM) machine, synchronous reluctance machine.**

I. Introduction

ELECTRIC vehicles (EVs) have emerged as a cleaner and sustainable choice in contrast with internal combustion engine vehicles (ICEVs). It helps in reducing the dependence on finite resources like fossil fuels, and is considered as a significant step toward a greener environment and in mitigating air pollution. Permanent magnet synchronous motor (PMSM) is a class of widely used traction motor in EVs, considering their high efficiency and power density [1], [2], [3]. The design of the same is a highly researched area [2], [4], [5]. They utilize rare-earth permanent magnets (PMs), with high energy density, in their rotor, resulting in lesser losses and better power factor. However, the high price of rare-earth magnets causes notable impact on the machine cost [6]. Hence, there has been a growing interest in synchronous reluctance machines (SynRM), known for their affordability, and simple construction [7], [8]. Unlike PMSM, the rotor of a SynRM does not produce or induce any magnetic field, rather it generates torque due to the tendency of the magnetic flux to flow through the path which has the lowest reluctance. Due to the absence of magnets, the torque density and power factor of SynRM is lower than that of PMSM [6], [9]. These shortcomings are compensated by placing magnets (generally ferrite PMs or rare-earth PMs of low volume) in the rotor, forming what is called a permanent magnet-assisted synchronous reluctance machine (PMaSynRM) [10], [11]. PMaSynRM is a hybrid of PMSM and SynRM. There are two components of torque in a PMaSynRM, one contributed by the reluctance of the rotor, other by the magnets. Unlike interior permanent magnet synchronous motor (IPMSM), which also has two torque components, in a PMaSynRM, the major component of torque is contributed by reluctance of the machine. Thus, this machine has the advantage of better torque density and efficiency than a SynRM, and better cost effectiveness when compared to a PMSM.

The constant power speed range (CPSR) is the ratio of maximum speed to base speed at constant power. A broad CPSR alongside a high maximum operating speed are essential criteria for an EV [12]. The CPSR needed for commercial passenger EVs typically falls between 4 and 7, while for heavy-duty direct drive electric trucks, it can reach up to 25 [13], [14]. Field weakening (FW) is a common technique used to extend the operating region of a PM machine. It is realized by sending demagnetizing current so as to bring down the air-gap flux, thereby increasing the machine speed in order to maintain back-EMF constant. Increasing dc bus voltage, adopting multiphase configurations,

Received 18 December 2024; revised 16 March 2025, 21 May 2025, and 29 July 2025; accepted 23 September 2025. Date of publication 1 October 2025; date of current version 19 January 2026. This work was supported by the Science and Engineering Research Board (SERB), Government of India, under Project CRG/2022/005535-G. Recommended for publication by Associate Editor T. Yang. *(Corresponding author: Veena Prasanna.)*

Veena Prasanna and Kamalesh Hatua are with the Department of Electrical Engineering, Indian Institute of Technology Madras, Chennai 600036, India (e-mail: ee19d208@smail.iitm.ac.in).

Kunal Layek is with the Department of Electrical and Computer Engineering, University of Illinois at Urbana-Champaign, Urbana, IL 61820 USA.

Color versions of one or more figures in this article are available at https://doi.org/10.1109/TPEL.2025.3616503.

Digital Object Identifier 10.1109/TPEL.2025.3616503

using dual 3-ϕ configurations [12] and winding switching [15] are some of the methods to obtain high CPSR. All these methods require additional stator current (FW current) in the high-speed operation, which adversely affects its efficiency [4]. For the case of PM machines, using winding change-over techniques like star-delta [16], series-parallel [17], unequal split [4], tapped [18], [19] etc., for obtaining increased speed range, requires the usage of additional bidirectional switches which adds to the overall size, losses, and complexity.

Multipole machines viz. Hunt motor have been mentioned in the literature of IMs, where it is used in the speed control of the same [20]. There exists two independent rotating magnetic fields (RMF) in the air gap sharing a common magnetic path. In [21], the conditions for arranging two sets of 3-ϕ windings corresponding to each pole number, in order to eliminate mutual interaction, are given. However, the objective of the machine is to control the speed by combined operation and not to perform any winding change-over based speed range extension.

This article discusses a synchronous machine which has two RMFs in the air gap. These fields are created by two different pole structures which are in the ratio of 1:3 (n pole and $3n$ pole). The n pole machine is formed by the synchronous reluctance component and the $3n$ pole machine is constituted by PMs. While the descriptions apply to any n pole-$3n$ pole machine, a 4-pole-12-pole machine is specifically discussed from this point onwards. The rotor is designed to work as both a 4-pole SynRM and a 12-pole Surface Mount PMSM (SMPMSM).The stator has two sets of 3-ϕ windings, one for each of the two rotor kinds. They are excited from two inverters which share the same dc bus. The supplying frequencies of each winding sets are in the ratio of 4:12, in order to produce a steady torque. Hence, the proposed machine operates as sum of two machines, viz. SynRM and PMSM. Thus, while the proposed machine resembles a PMaSynRM by producing torque through both permanent magnet and reluctance components, it differs from the conventional PMaSynRM due to its multiple pole configuration. Therefore, it is termed as multipole PMaSynRM.

At low speed, both machines are excited, whereas above an intermediate speed, only the PMSM is excited.

The machine is designed so that the base speeds of each component are different. The base speed of SynRM is chosen as that of the required rated speed, whereas the base speed of PMSM is chosen as the maximum speed of the requirement. Since the base speed of PMSM is the maximum speed, the operation at high speed is the below base speed operation of PMSM, eliminating FW. In general case, to achieve higher speeds, FW region exists and a major component of current is utilized in supporting the voltage (i_{sd}) and only the rest is utilized for producing torque (i_{sq}). This leads to a significant decline in efficiency at high speeds. The proposed machine completely eliminates FW operation at higher speeds, thereby utilizing inverter current more effectively, which results in better efficiency.

The operation of the proposed machine along with the control architecture is explained in Section II of this paper. Section III provides the complete design process of both stator and rotor. Section IV presents the analysis results which validate the proposed concepts of this article.

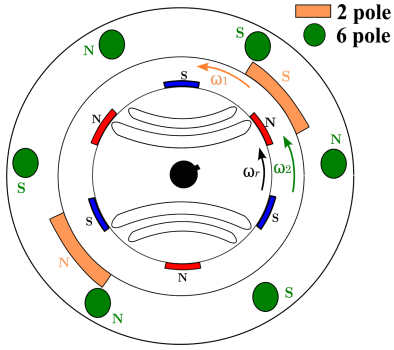

Fig. 1. Arrangement of 2 pole-6 pole structure.

II. Proposed 1:3 Multipole PM Assisted SynRM Operation

In this section, the operating principle and the operation of the proposed multipole PMaSynRM are discussed.

A. Operating Principle

In the proposed machine, a single rotor arrangement contains both a 4-pole salient structure and a 12-pole PM structure. The stator houses two sets of 3-ϕ windings corresponding to 4-pole and 12-pole. To produce a steady torque, the two RMFs should be rotating at the same mechanical speed, which is achieved by exciting the winding sets with currents whose fundamental frequencies also vary in the same ratio (4:12).

Theoretically, if the windings are distributed sinusoidally and the air-gap flux density consists only of the fundamental corresponding to 4-pole and 12-pole, then there will be no interaction between them. Practically, due to slot harmonics and winding distribution, there exists some interaction between them. Nevertheless, the back-EMFs induced in the SynRM windings due to PM and vice-versa, are negligible. This fact enables it to be regarded as the combination of two machines.

In Fig. 1, a simple 2 pole-6 pole structure is graphically presented for the purpose of conceptual understanding. From the figure, it can be observed that the magnet poles, the rotor saliency, and the poles created by the RMFs are in synchronism. Hence, there is no relative motion between the RMFs, thus producing only steady torque and avoiding the generation of any ripple torque in the process.

Here, ω_1, ω_2, and ω_r are the mechanical speeds of 2-pole RMF, 6-pole RMF, and rotor speed in rad/s, respectively. For steady torque operation,

$$\omega_1 = \omega_2 = \omega_r. \tag{1}$$

B. Operation

The power circuit of the proposed machine is illustrated in Fig. 2. The two voltage source inverters (VSI) operate independently to energize their respective winding sets. Despite the presence of two components, namely SynRM and PMSM, decoupled operation is achievable due to the asymmetry of the poles.

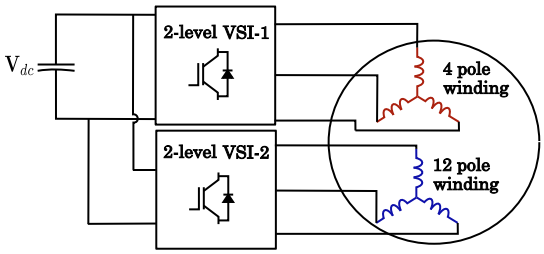

Fig. 2. Power circuit of the proposed machine.

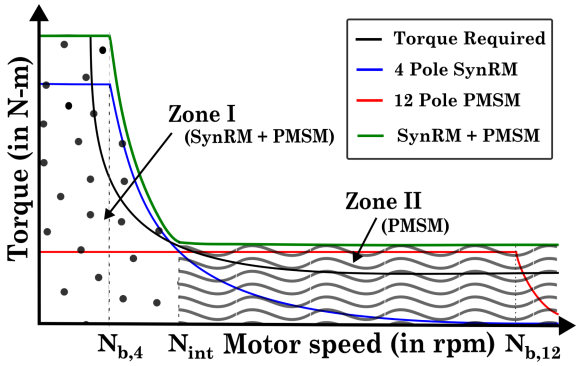

Fig. 3. Required torque versus speed characteristics and the proposed machine characteristics.

Fig. 3 illustrates the requirements and how the proposed machine operates to satisfy them, where $N_{b,4}$ and $N_{b,12}$ are the base speed of reluctance and PM components, respectively, and N_{int} is the intermediate speed. In a conventional PMaSynRM, the major component of torque is contributed by the reluctance component and the rest by PMs. This also occurs in the proposed multipole PMaSynRM during the combined operation, where SynRM contributes a larger portion of the torque compared to PM (say, $T_{SynRM} \approx 4\,T_{PM}$).

The operation of the proposed machine can be classified into the following regions:

1) *Below intermediate speed:* $0 \leq N \leq N_{int}$*:* In this region, both reluctance component and magnet component windings are excited. The torque is the resultant of reluctance torque of the 4-pole system and magnet torque of the 12-pole system. The reluctance component may enter into the FW region of the same, whereas the magnet component remains in its respective below base speed operation.
2) *Above intermediate speed until maximum speed:* $N_{int} \leq N \leq N_{b,12}$*:* In this region, the reluctance component windings are deactivated. As a result, only the magnet part contributes to the torque. The magnet component continues to be in its below base speed operation.

The 4-pole SynRM windings are not impacted by the 12-pole PMSM windings, by virtue of different pole combinations. The corresponding mathematical derivation is presented as follows.

The flux linkage of any 4-pole coil (of span $\frac{\pi}{2}$ mechanical radians) due to the flux density of 12-pole PM is expressed as (2). Here, r and l denote the air-gap radius and stack length of the machine, respectively, and B_m denotes the peak air-gap flux density due to PM

$$\Phi_{1,PM} = \int_{\phi_s}^{\phi_s+\frac{\pi}{2}} B_m \sin 6(\phi_s - \theta_r) r l d\phi_s. \tag{2}$$

The total flux linkage of the winding N_{a1}, due to the PM is calculated using

$$\lambda_{PM,a1} = \int_{<\frac{\pi}{2}>} -\frac{N_{a1}}{4} \sin\phi_s \left[\int_{\phi_s}^{\phi_s+\frac{\pi}{2}} B_m \sin 6(\phi_s - \theta_r) r l d\phi_s\right] d\phi_s \tag{3}$$

where N_{a1} is the turns per phase of phase R_4, ϕ_s is the stator angle with respect to the R_4 axis (α-axis) and θ_r is the angular displacement of the rotor with respect to the R_4 axis. The expression (3) is evaluated to be zero, proving that the PM flux linkage in the SynRM winding is absent. Fig. 4 shows the quadrant of the stator and rotor configuration of the 4-pole-12-pole machine.

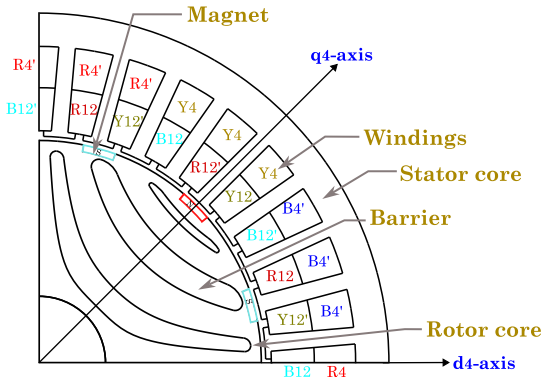

Fig. 4. Quadrant of the proposed 4-pole-12-pole machine.

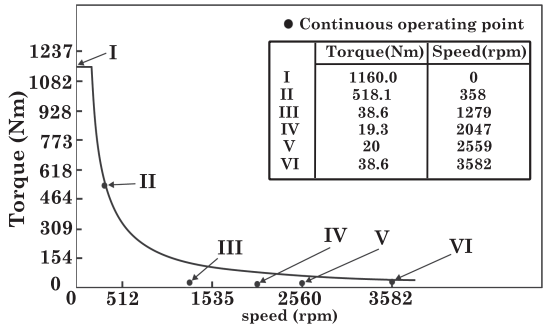

Fig. 5. Torque versus speed curve of heavy-duty truck.

C. Comparison With Conventional 3-ϕ PMaSynRM

The benefits of the proposed machine for EV applications, in comparison to a conventional 3-ϕ machine, are illustrated through a case study involving a heavy-duty truck, with torque-speed requirements derived from [22]. This is represented graphically in Fig. 5.

A comparative analysis is conducted between a 4-pole PMaSynRM and the proposed 4-pole-12-pole PMaSynRM, both

TABLE I
REQUIREMENTS OF THE MOTOR

Parameter	Value
Rated power	18.6 kW
Base torque	1160 Nm
Base speed	153 rpm
CPSR	24.7
Maximum speed	3780 rpm
Torque at maximum speed	47 Nm

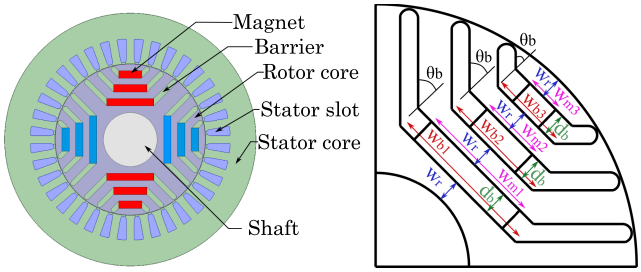

Fig. 6. (a) 4-pole PMaSynRM (M_1). (b) Rotor structure of M_1 with various dimensions marked.

TABLE II
VARIOUS DIMENSIONS OF M_1 AND M_2

Parameter	Symbol	Value
Stator outer diameter	D_{so}	688 mm
Stator inner diameter	D_{si}	413 mm
Rotor outer diameter	D_{ro}	411 mm
Shaft diameter	D_{sh}	147 mm
Stack length	l	229 mm
Air-gap	g	1 mm

of which meet these operating conditions. Henceforth, the designed conventional 3-ϕ 4-pole PMaSynRM is referred as "M_1," whereas the proposed multipole (4-pole-12-pole) PMaSynRM is referred as "M_2." The requirement of the machine is outlined in Table I.

Both machines are designed under the assumption that

1) the main dimensions remain the same;
2) the number of slots remain the same;
3) total number of conductors remain the same;

1) 18.6kW, 4-Pole PMaSynRM Design (M_1): A conventional PMaSynRM features boat-shaped flux barriers, within which rectangular permanent magnets are embedded [23], [24]. The designed conventional 4-pole PMaSynRM, which satisfies the requirement given in Table I, is shown in Fig. 6(a). The various dimensions of the design are provided in Table II. The stator design is identical for both M_1 and M_2.

The various geometrical parameters of the rotor are marked in Fig. 6(b) and presented in Table III. The iterative design process is followed according to [25], until the torque requirement is met at the base speed. Further, the CPSR requirement is met by varying the dc bus voltage. Table IV presents various parameters of M_1.

2) 18.6kW, 4-Pole-12-Pole PMaSynRM (M_2): The 4-pole-12-pole PMaSynRM, which satisfies the requirements given in Table I, is shown in Fig. 7(a). The dimensions are kept the

TABLE III
GEOMETRICAL PARAMETERS OF ROTOR OF M_1

Parameter	Symbol	Value
Insulation ratio	k_{air}	0.45
Radial rib	w_r	18.14 mm
Barrier width 1	w_{b1}	128.32 mm
Barrier width 2	w_{b2}	89.83 mm
Barrier width 3	w_{b3}	62.88 mm
Magnet width 1	w_{m1}	53.88 mm
Magnet width 2	w_{m2}	29.17 mm
Magnet width 3	w_{m3}	18.59 mm
Magnet depth	d_b	19.79 mm
Barrier angle	θ_b	45°

TABLE IV
PARAMETERS OF M_1

Parameter	Symbol	Value
DC bus	V_{dc}	1300 V
Number of slots	Q_s	36
Conductors per slot	z_u	28
Saliency ratio	ρ	7.6
PM flux linkage	Ψ_m	0.64 Wb
$d-$axis inductance	L_d	0.040 H
Phase current RMS	I_{rated}	47 A

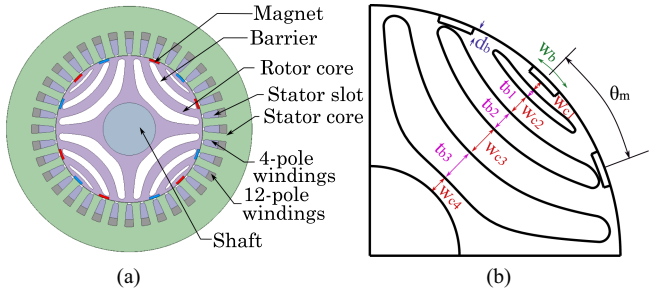

Fig. 7. (a) 4-pole-12-pole PMaSynRM (M_2). (b) Rotor structure of M_2 with various dimensions marked.

same as that of M_1 as given in Table II. The design of 4-pole reluctance part is performed with a three barrier structure. Since the number of slots remains the same, which is 36, the slots per pole pair becomes 18 for 4-pole structure. Thus, the number of separation points per pole pair, n_r, could be 14 or 22. The design process of multipole machine is explained in detail in Section III. Using Finite-Element Analysis (FEA), the structure which results in the highest ratio of average torque to torque ripple is obtained. The geometrical parameters of the rotor are shown in Fig. 7(b), and are presented in Table V. Table VI presents various parameters of M_2.

3) Comparison of M_1 and M_2: The designed machines in the previous sections, shown in Fig. 8, are capable of delivering the required power for the same application. However, the requirements for phase current, dc bus voltage, and magnet volume are different, which is discussed based on the parameters of the machine tabulated in Tables IV and VI.

In M_1, the PM and the reluctance component share the same number of poles. However, in M_2, the 4-pole windings do not contribute to the PM flux linkage. Consequently, the base torque of M_2 is lower than that of M_1. To achieve the same base

TABLE V
GEOMETRICAL PARAMETERS OF ROTOR OF M_2

Parameter	Symbol	Value
Insulation ratio	k_{air}	0.45
Carrier width 1	w_{c1}	6.93 mm
Carrier width 2	w_{c2}	19.44 mm
Carrier width 3	w_{c3}	28.09 mm
Carrier width 4	w_{c4}	15.59 mm
Barrier width 1	t_{b1}	7.70 mm
Barrier width 2	t_{b2}	19.63 mm
Barrier width 3	t_{b3}	29.98 mm
Magnet width	w_b	30 mm
Magnet depth	d_b	5.7 mm
Magnet center angle	θ_m	25°

TABLE VI
PARAMETERS OF M_2

Parameter	Symbol	Value
DC bus	V_{dc}	340 V
Number of slots	Q_s	36
Conductors per slot of 4-pole	z_{u4}	24
Conductors per slot of 12-pole	z_{u12}	4
Saliency ratio of 4-pole SynRM	ρ_4	7
$d-$axis inductance of 4-pole	L_{d4}	0.045 H
PM flux linkage of 12-pole PMSM	Ψ_m	0.09 Wb
$d-$axis inductance of 12-pole	L_{d12}	0.001 H
Saliency ratio of 12-pole PMSM	ρ_{12}	1
Phase current RMS	I_{rated}	56 A

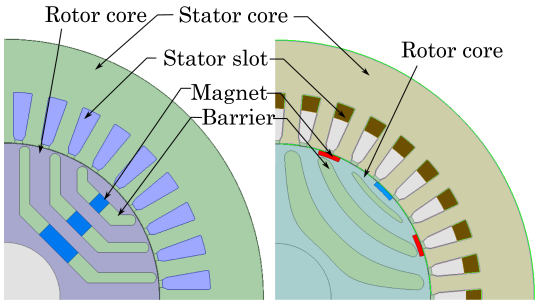

Fig. 8. M_1 and M_2.

TABLE VII
COMPARISON IN TERMS OF DESIGN PARAMETERS

Parameter	M_1	M_2
p.u Magnet volume	1	0.25
DC bus	1300 V	340 V
Phase current RMS	47 A	56 A
kVA rating	64.8 kVA	40.4 kVA

torque while maintaining the same number of conductors, M_2 requires a higher current compared to M_1 . This is evident in the observations presented in Table VII. After finalizing the base torque design, the dc bus is selected which could cover the torque requirements at the maximum speed. The torque requirement of 38.66 N · m at 3582 r/min is met when the dc bus is increased to 1300 V in the case of M_1. The high value of dc bus becomes a characteristic requirement of three-phase drives, which demands wide CPSR, such as the case of heavy duty trucks. From Table VII, a significant reduction in dc bus voltage and magnet volume is observed in M_2 relative to M_1.

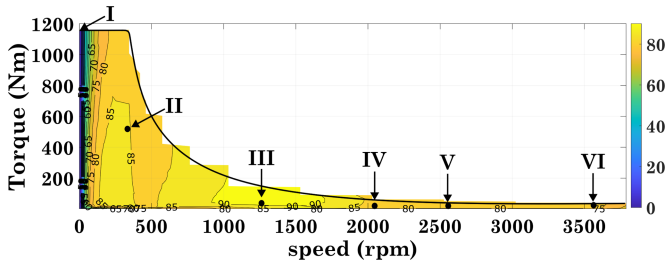

Fig. 9. Efficiency curve of 4-pole PMaSynRM .

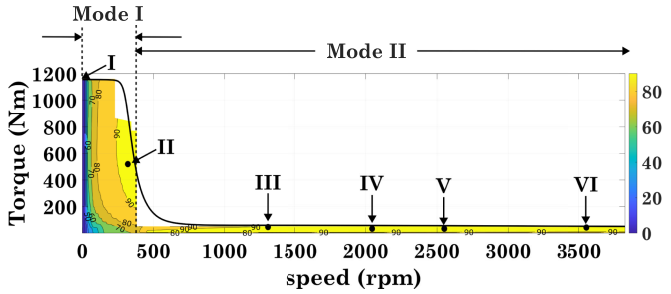

Fig. 10. Efficiency curve of 4-pole-12-pole PMaSynRM .

The magnet volume is reduced by 75% in M_2, as the magnets are designed solely to meet the torque requirements at high speeds. Since the required torque at these speeds is low, a smaller magnet volume suffices. The dc bus voltage also reduced by 73.8%. This also reduces the cost of associated capacitors, insulation levels of the components, and the switch voltage ratings.

Although the proposed topology uses two VSIs, the total KVA rating of the inverters for M_2 is lesser than M_1, owing to the low value of dc bus for M_2. The required voltage, current, and kVA ratings for M_1 and M_2 are summarized in Table VII. The presence of two inverters also adds to redundancy which supports higher reliability as in the event of failure of one inverters the drive still functions at a partial capacity.

The efficiency curve of M_1 is plotted with the envelope as the torque-speed characteristics and is provided in Fig. 9.

The efficiency curve of M_2 with the envelope as the torque-speed characteristics and is provided in Fig. 10. For the given application, after the operating point II, the torque requirement drastically falls. The required torque at 358 r/min is 518 N · m, whereas at 1279 r/min, it is 38 N · m. The intermediate speed is therefore selected to be slightly above 358 r/min, and is set at 460 r/min. Mode I is the region from start till intermediate speed, where both 4-pole and 12-pole windings are excited. From intermediate speed till maximum speed, only 12-pole windings are excited as is marked as Mode II in Fig. 10.

Apart from the constructional features and drive ratings which supports lower initial cost for the proposed machine, another major advantage of the proposed multipole PMaSynRM is the increment in the efficiency at high speeds, which supports lower operating cost of the drive. A table comparing the efficiencies of M_1 and M_2 at different operating points is provided in Table VIII. This occurs due to the reduction in copper losses because at high speeds, the 4-pole windings are not energized.

TABLE VIII
COMPARISON IN TERMS OF EFFICIENCY BETWEEN M_1 AND M_2

Operating point	Speed (rpm)	Torque (Nm)	η of M1	η of M_2	% increase in η
I	0	1160	NA	NA	NA
II	358.289	518.13	88%	93%	5.68%
III	1279.6	38.66	90%	93%	3.33%
IV	2047.37	19.33	76%	93%	22.36%
V	2559.21	20	80%	94%	17.5%
VI	3582.89	38.66	84%	95%	13.1%

While the quantitative advantages of M_2 over M_1 are discussed so far, in general, the advantages of the proposed topology over conventional 3-phase drives with common pole configuration for wide speed range applications can be summarized as under.

1) *Reduction in FW operation:* For applications requiring very high CPSR, 3-ϕ SynRM or PMSM machine, if designed for a low value of base speed, will have to operate largely in the FW region. This will incur more copper loss, owing to the high current requirement. The high FW requirement inversely affects magnet performance due to the risk of irreversible demagnetization [26]. To eliminate major FW operation, the machine has to be designed for high base speed, which will increase the drive size. In the proposed machine, the combined operation occurs only till an intermediate speed, where the SynRM component enters the FW operation. This intermediate speed is chosen to be slightly above the base speed of SynRM component, after which it shifts to the below base speed operation of PM component, thereby eliminating the FW operation.
2) *Elimination of bidirectional switches:* At intermediate speed, the excitation of SynRM windings need to be removed. In a pure reluctance machine, excitation can be removed without the need for switches. However, in a PM machine, switches are necessary for changeover operation due to the presence of nonzero back-EMF generated by the PMs. Consequently, in a conventional PMaSynRM, high-speed operation with winding changeover necessitates switches. However, in the proposed machine, the back-EMF induced in the reluctance windings due to PM is negligible, allowing them to be de-energized without switches. If this topology is compared with tapped or equivalent winding change-over schemes, the additional requirements of change-over switches are eliminated.
3) *Reduction in DC bus voltage:* The proposed topology can harness the benefits of winding change-over systems and reduce the effective number of turns at high speeds to suit the application requirements with lesser dc bus voltage rating compared to conventional 3-ϕ systems.
4) *Reduction in voltage rating of the components:* With the reduction in dc bus voltage, the voltage rating of the different components, viz. dc bus capacitors, inverter switches, etc., also reduce thus giving scope for cost reduction.
5) *Improvement in efficiency:* Since the effective number of turns are reduced at high speeds, the effective resistance also decreases, and hence for the rated current, the copper loss diminishes, improving efficiency.

TABLE IX
1.1-KW PROTOTYPE MOTOR REQUIREMENTS

Parameter	Value	Parameter	Value
P_{rated}	1.1 kW	V_{dc}	400 V
$\omega_{rated,4pole}$	1150 rpm	$\omega_{rated,12pole}$	8520 rpm
I_{rated}	7 A	T_{rated}	9 Nm
$T_{rated,SynRM}$	7.5 Nm	$T_{rated,PM}$	1.5 Nm

6) *Torque noninterruption:* In the conventional winding changeover schemes of PM-based machines, the changeover is characterized by a momentary torque interruption. In the proposed machine, this is eliminated by ensuring decoupling between the 4-pole and 12-pole windings.

D. Control Architecture

The decoupling is primarily between the 12-pole PM flux, which does not link the 4-pole SynRM winding. Hence, the control structure becomes significantly simple, as the two constituent motor counterparts can now be independently controlled. This decoupling also allows the control system to be designed in the respective rotor reference frame. This enables the currents injected from the SynRM and PMSM windings to be controlled to obtain their respective maximum torque per ampere (MTPA) conditions [27].

Both winding sets are independently controlled using standard field-oriented control (FOC) technique. A speed controller is designed to operate the machine, providing the torque reference. The torque and speed references are input into a look-up table (LUT), which determines the torque distribution. The resulting component torque references generate the corresponding d-q current references, which are then supplied to their respective current controllers. These controllers produce voltage references that are fed into the corresponding VSIs. The current references are expressed as a function of the rotor mechanical angle, and hence, a single position sensor is sufficient to control both the motor counterparts.

III. DESIGN PROCESS

The design process involves calculation of machine main dimensions, determination of magnet placement in the rotor and positioning the rotor barriers. In this section, the design procedure for a 4-pole-12-pole PMaSynRM is discussed. The design of a 1.1 kW, 400 V dc bus, 4-pole-12-pole PMaSynRM machine with requirements given in Table IX, using the proposed procedure, is also presented.

A. Main Dimensions

The machine main dimensions include stator outer diameter, stator inner diameter, rotor outer diameter and stack length.

The base speed of the proposed PMaSynRM is mainly determined by the SynRM component, which has 4-poles. Hence, the rated power of SynRM component is used to determine the main dimensions of the machine. The empirical relationship between machine volume and shaft power, P_{shaft}, is given by

$$P_{shaft} = C_{mech,4}\, D_{si}\, D_{ro}\, l\, n_{syn,4} \tag{4}$$

where $C_{mech,4}$ is the mechanical machine constant of the SynRM component, D_{si} is the stator inner diameter, D_{ro} is the rotor outer diameter, and $n_{syn,4}$ is the synchronous speed of the SynRM component. Since, the air gap being sufficiently small compared to the diameter of the machine, D_{si} is considered equal to D_{ro}. Here, the machine constant $C_{mech,4}$ is given as [28]

$$C_{mech,4} = \frac{\pi^2}{2}\, k_{w,4}\, \hat{A}_4\, \hat{B_{\delta,4}}\, \eta\, \cos\phi \tag{5}$$

where $k_{w,4}$, $\hat{A}_4$, and $\hat{B_{\delta,4}}$ represent the winding factor, the peak linear current density, and the peak air-gap flux density of the 4-pole SynRM component, respectively, η is the efficiency and $\cos\phi$ is the power factor.

Using (4) and the value of aspect ratio for synchronous machines given in [28], the main dimensions of the machine are established. In the case of 1.1-kW prototype machine, the values of $\hat{A}_4$, $\hat{B_{\delta,4}}$, η and $\cos\phi$ are chosen to be 25 kA/m, 0.4T, 0.9, and 0.8, respectively.

B. Stator Number of Turns Calculation

The stator parameters, such as stator slots, slot width, tooth width, and yoke width, can be designed similar to that of any 3-ϕ stator with distributed windings [28], [29]. The uniqueness in the design process of the proposed multipole PMaSynRM lies in the determination of winding topology which can create two sets of RMF in the air gap.

The slots will have two layers, each layer accommodating winding corresponding to each pole number. The calculation of pitch factor and distribution factor for each winding is the same as any 3-ϕ stator with distributed winding [29].

The reluctance component has lower base speed than the PM component. Hence, the number of turns are more in the reluctance windings.

Depending on the requirement, the base torque and the base speed of the 4-pole SynRM and 12-pole PMSM are fixed. From these values, the machine parameters for SynRM, viz. *d-q* axis inductances can be determined by choosing an inverter current limit and saliency ratio. In the case of PMSM, the parameters are calculated using normalized plots provided in [30], according to the given CPSR and power requirement. Therefore, the back-EMFs at the respective base speeds can be evaluated from the corresponding machine parameters. At the base speed of each component, the inverter reaches its limit. Thus, the inverter voltage limits for SynRM and PMSM are determined. However, since both windings are supplied from the same dc bus, the higher of the two calculated values is set as the final dc bus voltage. Hence, the number of turns can be calculated as the back-EMF developed at their respective base speeds is known.

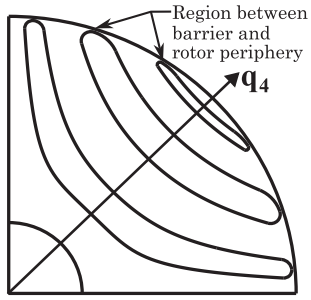

Fig. 11. Region between barrier and rotor periphery.

C. Rotor Design

The rotor design involves fixing the position of magnets on the rotor periphery and positioning the barriers appropriately so as to extract maximum torque with minimum ripple. The important factors to be considered while designing the rotor are as follows:

1) Although, theoretically, the back-EMF induced in the 4-pole windings due to 12-pole flux is zero (3), the nonsinusoidal nature of the winding distribution and the presence of slot harmonics may cause some interaction, which should be minimized.
2) The torque shared between 4-pole reluctance machine and 12-pole PM machine are satisfied according to the requirement.

Since the torque is contributed by two components consisting of two different pole numbers, each component of the rotor is considered separately for the design. The rotor design can thus be divided into two parts as follows:

1) Design of Reluctance Component: In a SynRM, the torque production primarily depends on the anisotrophy of the rotor structure. To facilitate the same, there are iron segments and air barriers in the rotor. Here, the axis of minimum inductance (maximum reluctance) is considered as the q_4-axis, about which the barriers will be symmetrical. The region between the barrier end and the rotor periphery is shown in Fig. 11. During operation, this region becomes saturated and serves as the transition zone between the magnetic potentials in the carriers. For ease of analysis, this region can be represented by a point on the rotor periphery. Such points are called separation points (SP). They represent the rotor iron ribs that become saturated due to the stator MMF, resulting in different magnetic potentials across the iron segments.. Thus, SPs act as the changeover points of magnetic potential. They also represent the intersection of center line of barriers on the rotor periphery and are used to position the barriers in the rotor core.

In this design, fluidic barriers are chosen considering that it offers better utilization of air-gap flux since the barriers are constructed along the path of flux lines as for a solid rotor. The saliency and inductance differences are thereby increased. For a synchronous reluctance machine with Q number of slots and p number of pole pairs, the number of SPs per pole pair in the

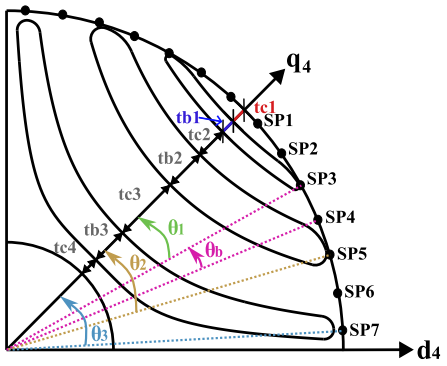

Fig. 12. Barrier and carrier width representation along with SPs for a 3-barrier 4-carrier SynRM.

rotor, in order to achieve minimum torque ripple, is given by [31]

$$n_r = \frac{Q}{p} \pm 4. \tag{6}$$

SPs are equally spaced, hence the angle between them can be obtained, as shown in Fig. 12, as

$$\theta_b = \frac{2\pi}{n_r}. \tag{7}$$

In the case of a 48 slot, 4 pole machine, n_r can be 20 or 28. The case when $n_r = 28$ is illustrated in Fig. 12. Here, there are 14 SPs per pole, which means 7 SPs on each side of the q_4-axis. Since SPs define the saturated region between the barriers and the rotor periphery, the number of SPs between the d_4- and q_4-axes corresponds to the number of possible barriers in the rotor. Hence, in this case, there can be a maximum of seven barriers possible, out of which three barriers are chosen and depicted in Fig. 12. Once the stator design is fixed, the performance of a reluctance machine primarily depends on the number of barriers and insulation ratio. A suitable number of barriers are chosen once the SPs are determined. It is observed that the average torque increases and torque ripple comes down as the number of barriers increases, but the increment is not profound at higher barrier numbers. The insulation ratio k_{air} is defined as the ratio of total thickness of barriers along q_4-axis to the sum of total thickness of barriers and q_4-axis iron in the rotor. For a 3-barrier rotor (see Fig. 12), k_{air} is defined as

$$k_{air} = \frac{t_{b1} + t_{b2} + t_{b3}}{t_{b1} + t_{b2} + t_{b3} + t_{c1} + t_{c2} + t_{c3} + t_{c4}} \tag{8}$$

where t_{bi} is the thickness of ith barrier, where $i = 1, 2, 3$, and t_{cj} is the thickness of jth carrier, where $j = 1, 2, 3, 4$. With the increase of insulation ratio, the power factor increases, but the average torque comes down. The value of k_{air} normally lies between [0.35,0.6] to achieve highest torque per ampere design [32].

The barriers are designed in such a way so as to reduce the q_4-axis flux, thereby increasing the difference between d_4-axis and q_4-axis inductance. The approach employed in this article relies on derivations provided in [32] and [33]. The width of each barrier can be calculated as follows:

$$t_{bi} = \left(\frac{D_{ro,synrm}}{2} - \frac{D_{ri}}{2}\right) k_{air} \frac{x_i}{x_{sum}} \tag{9}$$

where D_{ri} is rotor inner diameter or shaft diameter, $D_{ro,synrm}$ is the rotor outer diameter of synchronous reluctance component, which is given by

$$D_{ro,synrm} = D_{ro} - 2\,d_m \tag{10}$$

where d_m is the depth of magnet, which is given by (20). x_{sum} is given as

$$x_{sum} = \sum_{i=1}^{N_{bar}} x_i \tag{11}$$

where N_{bar} represents the number of barriers; x_i represents the intermediate variable and is given as

$$x_i = \Delta F_{qi} \sqrt{\theta_i}. \tag{12}$$

Here, θ_i is the angle of ith barrier from the q_4-axis. Fig. 12 illustrates the corresponding θ_i values for a three-barrier structure ($i = 1, 2, 3$). ΔF_{qi} represents differential MMF drop in p.u. across ith barrier along q_4-axis, and is given as

$$\Delta F_{qi} = F_i - F_{i+1} \tag{13}$$

where F_i represents average MMF in per unit (p.u.) seen by each barrier, and is given as

$$F_i = \frac{1}{\theta_i - \theta_{i-1}} \int_{\theta_{i-1}}^{\theta_i} \cos 2\theta \, d\theta. \tag{14}$$

The width of each carrier is made proportional to the flux flowing through them. The width of each iron part is given as

$$t_{ci} = \frac{(D_{ro,synrm} - D_{ri})\,(1 - k_{air})\,B_i}{2\,B_{sum}} \tag{15}$$

where B_i is the average flux density in p.u. in each carrier obtained by assuming sinusoidal flux density distribution in the air gap, and is given as

$$B_i = \frac{1}{\theta_i - \theta_{i-1}} \int_{\theta_{i-1}}^{\theta_i} \sin 2\theta \, d\theta. \tag{16}$$

The number of carriers, N_c, is given as

$$N_c = N_{\text{bar}} + 1. \tag{17}$$

For, $i = N_c$, (16) becomes

$$B_i = \frac{1}{\pi - 2\,\theta_{N_{bar}}} \int_{\theta_{N_{bar}}}^{\frac{\pi}{2}} \sin 2\theta \, d\theta. \tag{18}$$

B_{sum} is the sum of all average flux densities in p.u.

$$B_{sum} = \sum_{i=1}^{N_c} B_i. \tag{19}$$

Therefore, the barrier and carrier widths of the reluctance component can be established using (9) and (15) once the number of barriers and insulation ratio are fixed. The barrier and carrier width representation in the case of a 3-barrier rotor is also provided in Fig. 12.

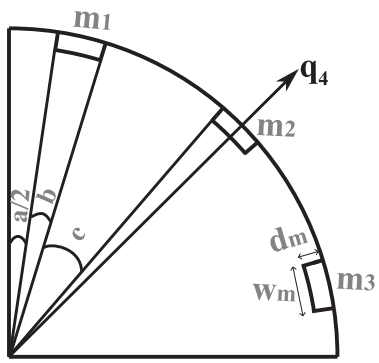

Fig. 13. Positioning of magnets and associated variables.

2) Positioning of Magnets: The magnets are placed on the rotor periphery so as to produce in the air gap only a 12-pole flux density, that is, a null 4-pole flux density, which is the fundamental flux density of this machine. Theoretically, the pole numbers are chosen such that there is no interaction between them. In such a case, the back-EMF induced in each winding of a corresponding pole number due to the other pole number would be null. But, practically, due to slot harmonics and winding distribution, the back-EMF induced due to the interaction between the pole numbers will not be zero.

The design process of the magnet component starts with determining the width and thickness of the magnet. First, the operating point of the magnet is fixed as the point which produces maximum energy density product $(BH)_{max}$, obtained from the B-H curve.

Let this point be considered as (B_m, H_m). The depth of magnet is given as

$$d_m = \frac{\hat{B_{\delta,12}}\, g}{\mu_0 H_m} \tag{20}$$

where $\hat{B_{\delta,12}}$ is the peak air-gap flux density of 12-pole PM component, g is air-gap length, and μ_0 is absolute permeability of air. The width of magnet is given as

$$w_m = \frac{\hat{B_{\delta,12}}\, w_g}{B_m} \tag{21}$$

where w_g is the width of air gap under one pole.

Once the width of the magnet is fixed, three magnets (m_1, m_2, and m_3) are placed along one pole of reluctance component as shown in Fig. 13.

The angle subtended by each magnet, in electrical degrees (4-pole as fundamental), is given by

$$b = 2\,\frac{2\,w_m}{D_{ro}}. \tag{22}$$

The relation between angle subtended by core in between magnets c and angle across d_{12}-axis a is given as

$$a + 3\,b + 2\,c = \pi. \tag{23}$$

The minimum value of c is zero. In order not to compromise the d_4-axis flux of reluctance component, the minimum value of a is taken as one slot pitch and the maximum value of c is taken as $\frac{a}{2}$, which gives

$$c_{\max} = \frac{\pi - 3\,b}{4}. \tag{24}$$

The magnets are placed above the flux barriers of the reluctance component in such a way that the 4-pole flux path will not be hindered. This can be made possible if the magnets are aligned with the SPs. The values of a and c can be found by an iterative process, which involves placing the magnets on each SPs and observing the variation of fundamental and major harmonics in normal air-gap flux density distribution. Since the PM represents 12-pole system, the values which result in minimum 4-pole component and maximum 12-pole component are selected, thereby fixing the magnet position.

TABLE X
1.1-KW PROTOTYPE MOTOR PARAMETERS

Parameter	Value	Parameter	Value
D_{so}	210 mm	D_{si}	136 mm
D_{ro}	134 mm	l'	100 mm
D_{ri}	40 mm	d_m	5 mm
w_m	10 mm	t_{b1}	2.2 mm
t_{b2}	7.9 mm	t_{b3}	7.0 mm
t_{c1}	1.9 mm	t_{c2}	7.1 mm
t_{c3}	10.9 mm	t_{c4}	5.8 mm

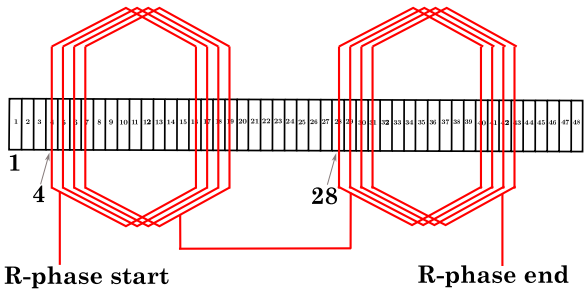

Fig. 14. R-phase of 4-pole winding.

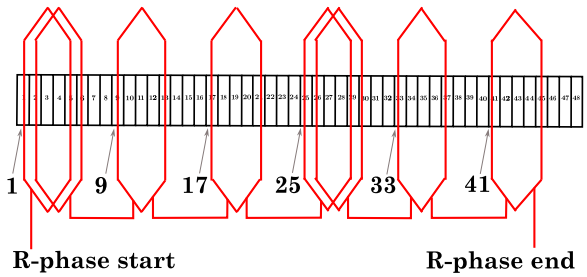

Fig. 15. R-phase of 12-pole winding.

D. Design of 1.1-Kw Prototype Motor

A 4-pole-12-pole prototype motor is designed, with its details provided in Table X.

For a 48 slot, 3-ϕ, 4-pole-12-pole machine, slot per pole per phase for 4-pole is $n_4 = 4$, resulting in an integral slot winding as shown in Fig. 14, and that of 12-pole is $n_{12} = 1.34$, resulting in fractional slot winding as shown in Fig. 15.

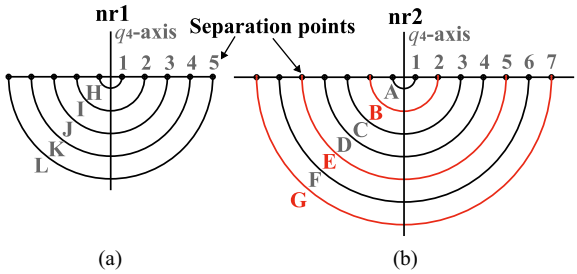

Fig. 16. Possible barriers and separation points.

TABLE XI
AVERAGE TORQUE OF 3-BARRIER SYNRM

Barriers	$T_{avg}(Nm)$	Barriers	$T_{avg}(Nm)$
ACF	3.39	BEF	4.04
ACG	3.06	BEG	4.21
ADE	3.07	BFG	4.20
HIJ	3.01	HKL	3.00
HIK	3.16	IJK	3.23

The rotor design process is described below.

1) Lower Pole Number: The lower pole number corresponds to the reluctance component of the machine. The design procedure of rotor starts with choosing the barrier position and determining the barrier dimensions. The calculation involves determining rotor outer diameter of reluctance component, which is given by (10).

The value of k_{air} is chosen to be 0.4. The number of SPs per pole pair in the rotor is given by (6). As explained in Section II-I-C, for the case of a 48 slot, 4-pole machine, the value of n_r is either 20 or 28. Consequently, the number of SPs per pole can be 10 (let this case be named n_{r1}) or 14 (let this case be named n_{r2}). Since the number of SPs between the d_4- and q_4-axes corresponds to the number of possible barriers in the rotor, there can be five barriers in the case of n_{r1} and seven barriers in the case of n_{r2}. Fig. 16(a) represents the case of n_{r1}. The five barriers of n_{r1} are represented using the alphabets H, I, J, K, and L. They are drawn as semicircles for representation purpose only and has no relation to the shape of the barriers. Similarly, Fig. 16(b) represents the case of n_{r2}. The seven possible barriers for this structure are represented using the alphabets A to G. In both these figures, the SPs are represented using circles and the horizontal line corresponds to the unwrapped view of the rotor periphery. Taking into account the manufacturability of the design, the number of barriers is chosen to be 3. Using the principles of permutation and combination, three barriers can be chosen from five and seven barriers in ${}^5C_3$ and ${}^7C_3$ ways, respectively.

FEA is conducted to evaluate the torque, and some of the selected results are given in Table XI. Here, the combination BEG refers to the case of n_{r2} with the barriers corresponding to SPs 2, 5, and 7, as highlighted in Fig. 16(b).

The combination BEG achieves the maximum torque as a 4-pole SynRM. This establishes the lower pole design.

2) Higher Pole Number: The design of a higher pole number involves fixing the position of magnets such that maximum torque is generated while maintaining minimum interaction between the poles. For each pole of the 4-pole structure, 3 poles of 12-pole exist. These three poles are constituted by three magnets which are placed in an embedded fashion. Initially, the magnets are designed in a surface-mounted configuration and later embedded to enhance the structural stability. Since the air-gap flux density contributed by the magnets is significantly lower than that of the SynRM, their volume is relatively small. As a result, embedding the magnets does not notably affect their electromagnetic performance, and their saliency remains largely unchanged. The center magnet (m_2 in Fig. 13) is placed along the high reluctance axis of 4-pole (q_4-axis). The remaining two magnets (m_1 and m_3) are symmetrically positioned about the q_4-axis. The position of m_2 is fixed. Once the position of m_1 is set, the position of m_3 is automatically determined, and vice-versa. It is not possible forecasting which is the better layout of the magnets. To avoid disturbing the 4-pole flux, the analysis is performed as two cases, one by keeping the center of the magnet across each SP [see Fig. 17(a)], and second by keeping the center of the magnet across the center point of two adjacent SPs [see Fig. 17(b)]. Using FEA, the corresponding air-gap flux density is gained, and its Fourier coefficients are evaluated. Since the rotor structure with 14 SP per pole is chosen for the 4-pole SynRM, harmonic analysis is performed on the same. For some of the considered cases, Table XII reports the ratios b_3/b_1 and b_3/b_5, where b_1, b_3, and b_5 represents the Fourier coefficients of the normal air-gap flux density distribution (B_n) corresponding to fundamental (4-pole), third harmonic (12-pole) and fifth harmonic, respectively.

Table XII shows the analysis of the air-gap flux density produced solely by the magnets placed at various positions. Here, the term "Magnet position w.r.t. SP" denotes the location of the center of m_1 or m_3 relative to the SPs. The figures are the position of the magnet's center from the q_4-axis written in terms of SPs. This is illustrated in Fig. 18. For example, the value 4 corresponds to the situation when the center of m_1 (or m_3) lies on SP number 4, as shown in Fig. 18(a), and the value 4.5 corresponds to the situation when the center of m_1 (or m_3)

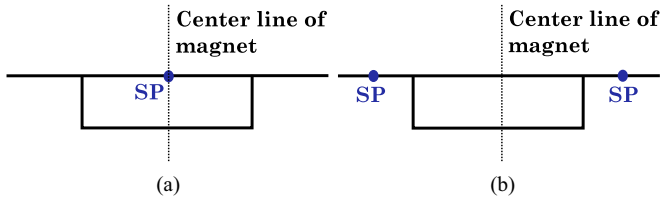

Fig. 17. Placement of magnet m_1 or m_3 where the center of the magnet coincides with (a) the center of SP (b) the center of two adjacent SPs.

TABLE XII
HARMONIC ANALYSIS OF AIR-GAP B_n WITH 14 SP PER POLE

Serial No.	Magnet position w.r.t SP	b_3/b_1	b_3/b_5
1	4.5	3.85	-1.54
2	5.0	7.06	-2.73
3	5.5	18.66	-7.69
4	6.0	-35.97	17.67

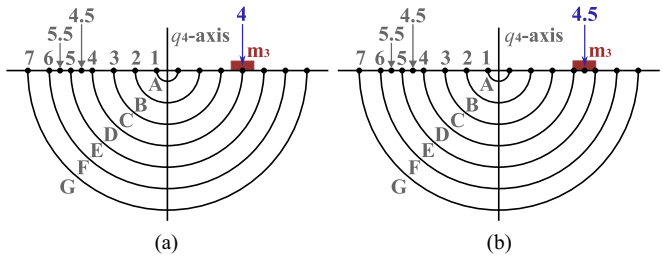

Fig. 18. Numbering of SPs where the center of the magnet is placed (a) at position 4 (b) at position 4.5.

lies at the mid-point between SPs number 4 and 5, as shown in Fig. 18(b). It is observed that values corresponding to Serial No. 3 in Table XII results in the maximum third harmonic content with minimal fundamental and fifth harmonic components. The corresponding values of a and c are 46° and 40°, respectively. This establishes the magnet position for a solid rotor with only magnets. When the rotor structure of lower pole number is joined with that of the higher pole number, modifications need to be made in the magnet position, as a part of optimization, so as to ensure better saliency. The magnets are aligned with the barrier ends such that 4-pole flux path is not hindered.

IV. Results

This section provides the details of the experimental arrangements and suitable simulation and experimental results.

A. Simulation Results

1) Electromagnetic Analysis: For the machine with specifications given in Table X, FEA is performed using ANSYS MAXWELL. The core material used is M43 electrical steel, which has a knee point flux density of 1.5 T, as obtained from ANSYS material library. The flux density distribution across all parts of the machine during MTPA operation at the base speed of SynRM (1150 r/min) is shown in Fig. 20. The current space vector which produces maximum torque for 4-pole component is marked as $\vec{I}_{4,MTPA}$. It occurs at an angle (β_4) of 48° *elec* from the rotor axis (d_4-axis), as observed from the simulation result in Fig. 23(c). The average torque contributed by 4-pole at this condition is 7.5 N · m, as observed in Fig. 23(a). The current space vector which produces maximum torque for 12-pole operation is marked as $\vec{I}_{12,MTPA}$. Since the saliency of 12-pole structure is 1, $\vec{I}_{12,MTPA}$ is aligned along the q_{12}-axis for maximum torque. At this condition, only q-axis component exists for $\vec{I}_{12,MTPA}$ which makes $i_{d12} = 0$, resulting in $\beta_{12,MTPA} = 90°$ *elec*. The average torque contributed by 12-pole at this condition is 1.5 N · m, as observed in Fig. 23(a). From Fig. 20, no significant saturation is observed.

In all the Fast Fourier Transform (FFT) analyses given in this section, harmonic order 1 corresponds to the 4-pole component, while harmonic order 3 corresponds to the 12-pole component. The analysis of the radial flux density established along the air-gap periphery by 4-pole current at its MTPA condition ($\vec{I}_{4,MTPA}$), with and without the presence of magnets, as shown in Fig. 19(a). From the corresponding FFT analysis given in Fig. 19(b), the presence of magnets have little to no effect on the 4-pole air-gap flux density. The analysis of the radial flux density along the air-gap periphery by the 12-pole magnets is shown in Fig. 19(c). Fig. 19(d) presents the FFT analysis of the same, it is found to have a fundamental (12-pole) peak of 0.1T, with negligible 4-pole component. The value 0.1T was chosen since the machine is designed for a low PM torque.

The flux density profile along the air-gap periphery, when both the winding sets are excited in their own respective MTPA points, is illustrated in Fig. 21(a). Fig. 21(b) shows the corresponding FFT profile. It is found to meet the desired fundamental values for the corresponding pole numbers, along with some undesirable higher-order harmonics, due to the presence of slots and fractional slot windings.

In Fig. 22(a), the flux linkage in 4-pole windings due to 12-pole PMs, is shown. From the corresponding FFT plot illustrated in Fig. 22(b), it is evident that the 12-pole PM has negligible influence on the 4-pole fundamental flux linkage. Therefore, the 4-pole component of the back-EMF induced in the 4-pole windings by the 12-pole is negligibly small in comparison to the rated inverter voltage. This enables the transition from combined operation to PM-only operation by deactivating the 4-pole windings, without the need for switches. The flux linkage in 12-pole windings due to 4-pole MMF, with and without the presence of magnets, is illustrated in Fig. 22(c). The corresponding FFT plot is provided in Fig. 22(d). From the profile, it is evident that the 4-pole MMF created minimal 12-pole flux linkage in the 12-pole windings when compared with that generated by the 12-pole magnets.

The torque profile during the combined operation of the 4-pole and 12-pole at their respective MTPA points, along with their individual contributions, at the base speed of the 4-pole, is presented in Fig. 23(a). The ratio of the shared torque between the 4-pole and 12-pole is 5. The combined torque is found to be the sum of individual components. The corresponding FFT plot is presented in Fig. 23(b). The ripple content is found to be below 10%.

Ideally, the proposed machine will achieve infinite speed if both winding sets remain continuously excited. However, in practice, the efficiency of SynRM may be low in its deep FW region. Hence, in such applications, an early cut off may be implemented as shown in Fig. 24. An intermediate speed of 4000 r/min is selected to demonstrate the operation. From starting till intermediate speed, both 4-pole and 12-pole windings are excited, which is represented as Mode I. At the intermediate speed, the excitation of 4-pole windings are removed, and until the maximum speed, only the 12-pole windings are excited which is represented as Mode II. The base torque of the combined machine is 9 N · m, where 7.5 N · m is contributed by SynRM and 1.5 N · m, by PMSM. The power-speed characteristics of the proposed machine is illustrated in Fig. 25. The power at the base speed of SynRM is found to be the same as the power at the base speed of PMSM, which are highlighted in red dashed lines. Hence, a CPSR of 7.4 is achieved.

The efficiencies at different torque and speeds of operation are enclosed within the envelope of the torque-speed capability of

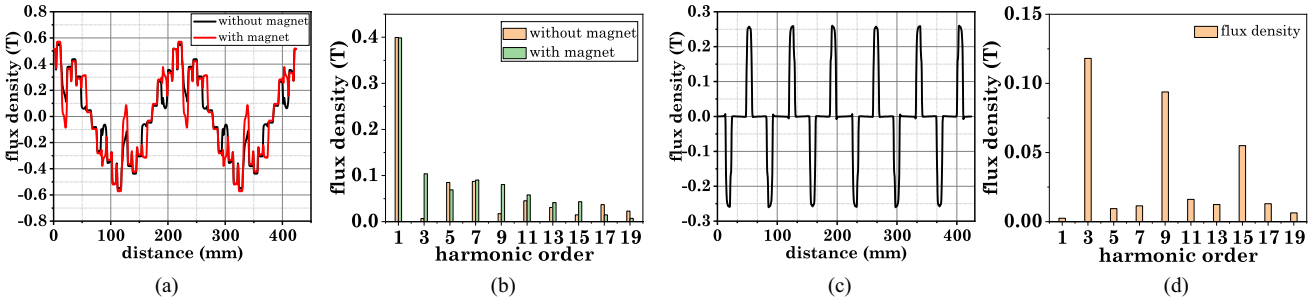

Fig. 19. (a) 4-pole air-gap B_n. (b) FFT of 4-pole B_n. (c) 12-pole air-gap B_n. (d) FFT of 12-pole air-gap B_n.

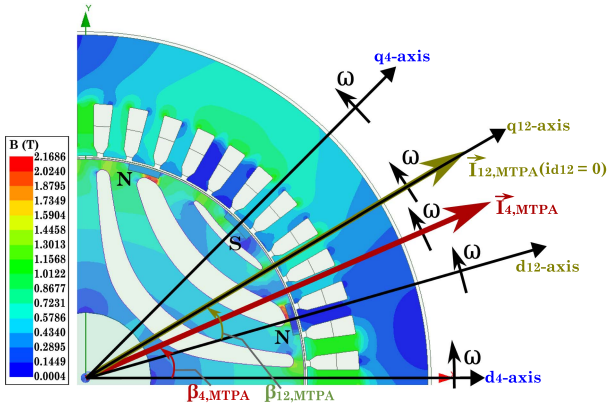

Fig. 20. Flux density distribution at 1150 r/min.

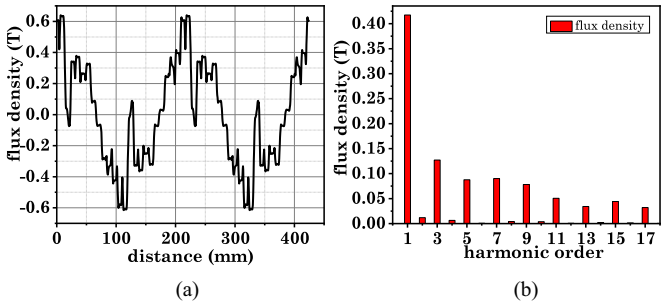

Fig. 21. (a) Air-gap B_n for combined operation. (b) FFT of air-gap B_n for combined operation.

the machine, and presented in Fig. 26. It is observed that at lower speeds, when both the windings are functional, the efficiency is comparatively less. This happens as at lower speeds, the power output is less, while the copper losses are the same as that of rated condition. This is a characteristic of all 3-ϕ machines. With increasing speeds, the efficiency is observed to improve. Above the intermediate speed, after the SynRM winding is de-energized, the effective resistance of the machine is reduced, thus reducing the copper losses. Hence, as described, the efficiency of the machine is observed to improve after cut off of the SynRM windings. This demonstrates the advantages of the proposed machine.

Further, the changeover operation is much easier in this machine category, as the SynRM windings do not develop any PM induced back-EMF. Hence, the changeover can be performed at any speed in the FW region, without allowing any uncontrolled regeneration. Therefore, additional switching circuitry for the changeover can be avoided.

TABLE XIII
MATERIAL PROPERTIES

Material	Property	Value[35]
M43 steel	Yield strength	270 MPa
	Tensile Ultimate Strength	460 MPa
	Density	7850 kgm^3
Magnet	Yield strength	285 MPa
	Tensile Ultimate Strength	460 MPa
	Density	7500 kgm^3

2) Demagnetization Analysis: The magnet is considered demagnetized when its operating point drops below the knee point of the normal magnetization curve. In the 4-pole–12-pole PMaSynRM configuration, the magnets are arranged in an embedded manner. Here, the 12-pole windings are energized such that the magnetic flux exclusively follows the q_{12}-axis for maximum torque production, from start till maximum speed. As a result, the risk of demagnetization is absent for a pure PMSM during operation below the base speed. However, since the 4-pole MMF is also present from start to intermediate speed, demagnetization analysis is conducted under these conditions. The magnetic field intensity along the path which pass through the center (d_{12}-axis) of each magnet is obtained using FEA and illustrated in Fig. 27.

The maximum demagnetizing field-intensity value is found to be 400 kA/m, which lies above the knee point as shown in Fig. 28, confirming absence of irreversible demagnetization.

3) Structural Analysis: In high-speed designs, centrifugal force is expected to be the primary cause of mechanical stress [34]. If the stress induced by the centrifugal force exceeds the maximum yield stress, the rotor undergoes permanent deformation. Therefore, FEA using ANSYS mechanical is performed to calculate the von-Mises stress developed throughout the rotor structure.

Table XIII lists the mechanical properties of the rotor materials. The rotor is subjected to a rotational velocity of 12 000 r/min and the stress distribution is analyzed. Figs. 29(a) and 29(b) illustrate the stress distribution of the rotor structure from the front and isometric views, respectively.

The stress causes deformation in the rotor. However, since the maximum stress observed is 191 MPa, which is below

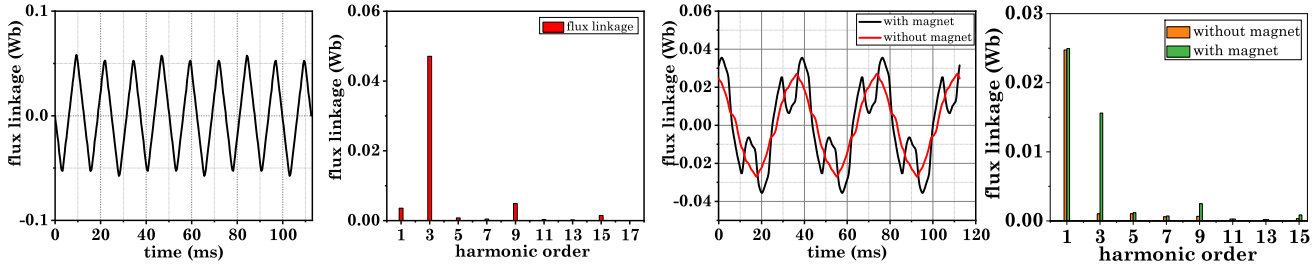

Fig. 22. (a) 4-pole flux linkage. (b) FFT of 4-pole flux linkage. (c) 12-pole flux linkage. (d) FFT of 12-pole flux linkage.

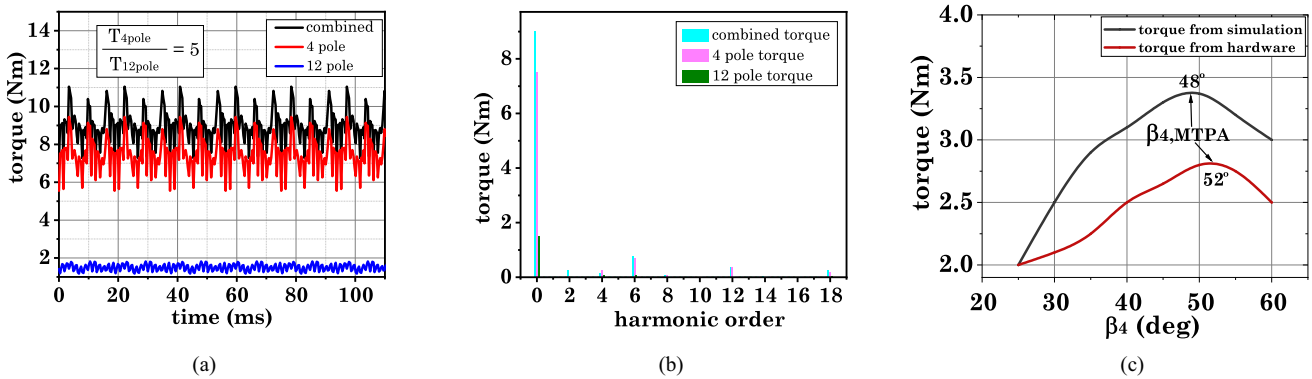

Fig. 23. (a) Torque profile at 1150 r/min. (b) FFT of torque at 1150 r/min. (c) Hardware and simulation result of torque versus β_4.

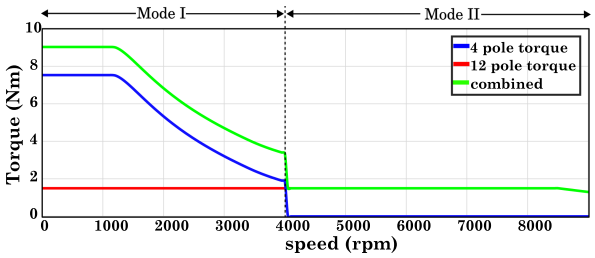

Fig. 24. Torque-speed curve when 4-pole windings are removed at 4000 r/min.

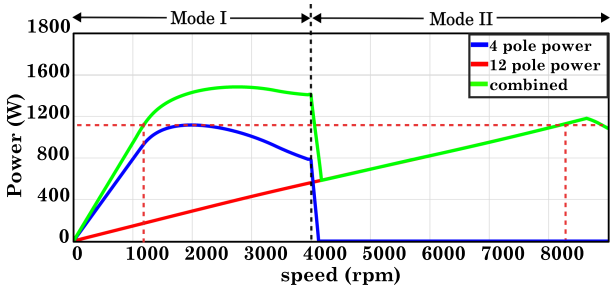

Fig. 25. Power-speed curve when 4-pole windings are removed at 4000 r/min.

the 270 MPa limit, irreversible deformation does not occur. The highest deformation, measuring 0.031 mm, occurs along the second carrier. The isometric view of the deformation is presented in Fig. 29(c).

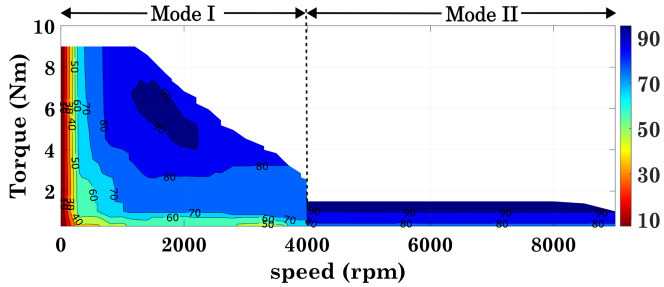

Fig. 26. Efficiency curve of the proposed machine.

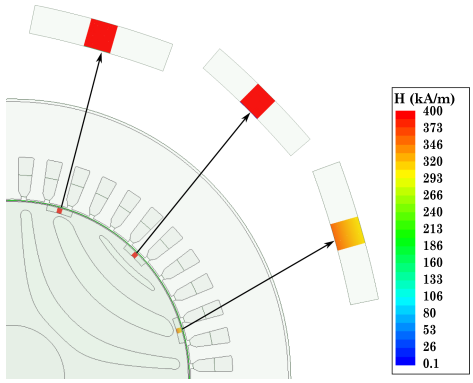

Fig. 27. Magnetic field intensity along d_{12}-axis of magnets.

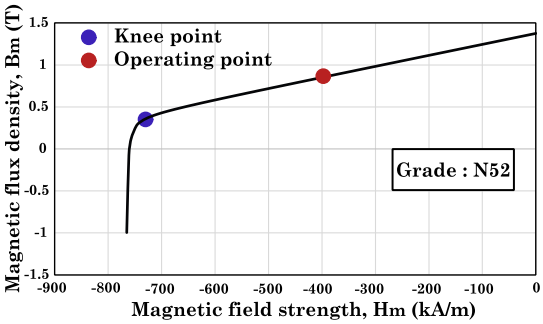

Fig. 28. Operating point of the magnet.

The stress values are within limits and the deformation is negligible relative to the 1 mm air-gap length.

B. Experimental Setup

A prototype 1.1-kW multipole PMaSynRM, as designed in this article, has been manufactured for experimentation. The manufactured rotor of the machine is shown in Fig. 30(c). The motor is mechanically coupled to an induction machine (IM), which acts as a load. The motor-load setup is provided with a torque transducer for precise measurement of torque. The motor-load setup is presented in Fig. 30(a).

The prototype multipole PMaSynRM is driven by two Si-IGBT-based VSIs. An image of the inverters with their accessories is presented in Fig. 30(b). The VSIs are controlled using a digital signal processor (DSP) manufactured by Texas Instruments (Model: TI TMS320F28335). The switching frequencies of the Si-IGBT switches are 10 kHz. FOC is implemented from both the VSI sides to extract the required steady torque from the machine.

C. Experimental Results

In this section, the experimental validation of the proposed concepts is presented. The test result of torque versus β_4 is shown in Fig. 23(c). It deviates from the simulation values due to inaccuracies in the manufacturing process.

1) Experimental Verification of Various Operating Modes: The operational concept of the proposed machine is demonstrated as follows:

1) Both winding sets energized: The operation below the intermediate speed is illustrated in Fig. 31(a). In this result, both VSI currents are injected as per the MTPA condition. The current pertaining to the 4-pole winding is captured in Ch4, and that of the 12-pole winding is captured in Ch2. To understand the operation of the machine in terms of the operating frequencies of the currents and the mechanical speed, Ch3 records the mechanical angle of the rotor, and it can be observed that for a single mechanical cycle, the SynRM currents complete two cycles (confirming 4-pole operation), and the PMSM completes six cycles (corresponding to 12-pole operation).
2) Torque output: The torque of the machine is recorded using a torque sensor and presented in Fig. 31(b). The torque sensor delivers a current output corresponding to the torque of the machine, which is measured using a signal conditioning circuit. The overall gain of these circuits is calculated, and the torque scaling is presented in the result to be 2.08 N · m/division of the scope, and hence, the torque output can be calculated to be approximately 8.5 N · m. Below the base speed, the rated current in both windings contributes toward torque production based on the MTPA condition of each motor counterpart. The base speed for the manufactured prototype is obtained at 1100 r/min, as can be inferred from the frequency of the currents pertaining to the 4-pole SynRM winding (Ch4) in Fig. 31(b). The filtered version of the applied line voltage from the VSI-1 (meant for 4-pole SynRM) is presented in Ch2 of Fig. 31(b). From the line voltage peak of approximately 300 V, the per-phase voltage can be calculated to be approximately 175 V. This value is 90 % of the maximum voltage available from the 2-level VSI using the Sine PWM technique (as $V_{dc} = 400\ V$), and is considered to be the voltage limit for the drive. Hence, this speed of 1100 r/min is considered the base speed.
3) Change-over operation: Another unique feature of this topology is the seamless and simple change-over technique. As discussed in the introduction, for the winding change-over of PM-based machines, a current overload is required for providing demagnetizing MMF during the change-over. However, the proposed machine has magnetically decoupled 3-ϕ winding sets. Thus, to perform change-over, the winding currents of SynRM winding are simply removed. These sequences of events are presented in Fig. 31(c). It is observed that the sudden turn OFF of SynRM pulses does not produce any uncontrolled current spikes (Ch. 4). The PMSM currents (Ch. 3) also do not experience any transient currents. Thus, the change-over technique allows seamless change-over without any torque interruption. It may be noted that the proposed topology does not impose any restriction on the selection of the change-over speed. Ideally, the SynRM winding can be operated till infinite speed, but in practice, in the deep FW region, the torque and the power output reduce drastically, and hence, for the sake of efficiency, the 4-pole winding is cut off. In the experimental results, the speed chosen for the cut off is 800 r/min. The seamless cut off can be obtained by virtue of the decoupling of the PM rotor flux with the 4-pole stator winding. This is confirmed from the voltage waveform (Ch1) of Fig. 31(c), where the back-EMF is negligible. The absence of any current spike ensures a safe change-over process.
4) High-speed operation: One of the advantages of the proposed machine is its decoupled operation, which allows the removal of the high torque winding at high speeds, and no additional switches are required to isolate the section of the winding. While the results for change-over is provided at 800 r/min, to ensure that the back-EMF of 4-pole winding from the PM induced flux is negligible even at higher speeds, the back-EMF of the SynRM winding is captured at 1500 r/min and presented in Fig. 32.

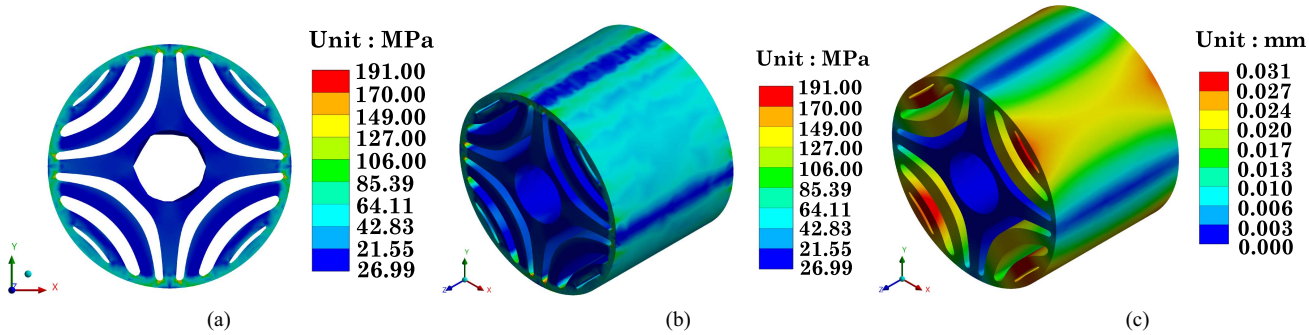

Fig. 29. (a) Front view of stress distribution. (b) Isometric view of stress distribution. (c) Isometric view of deformation distribution.

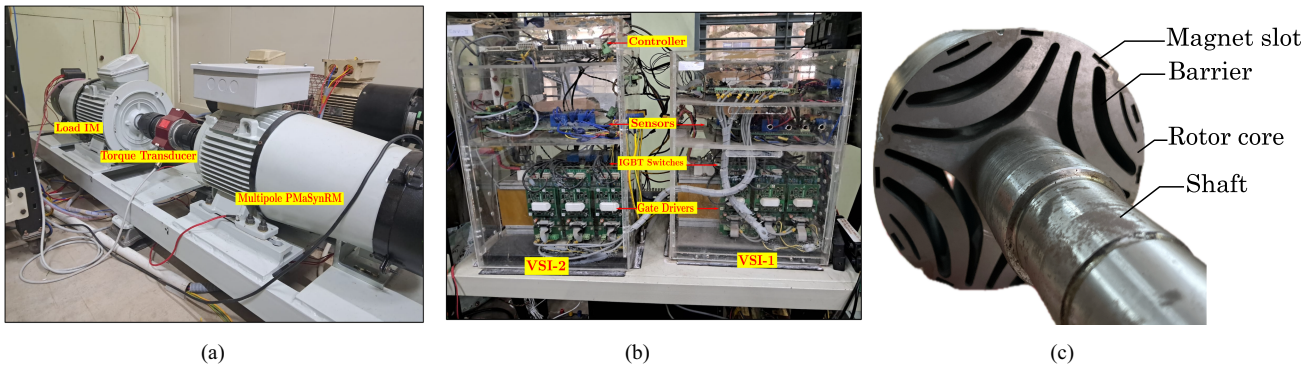

Fig. 30. (a) Experimental motor test arrangement. (b) VSIs for multipole PMaSynRM. (c) Manufactured rotor of the machine.

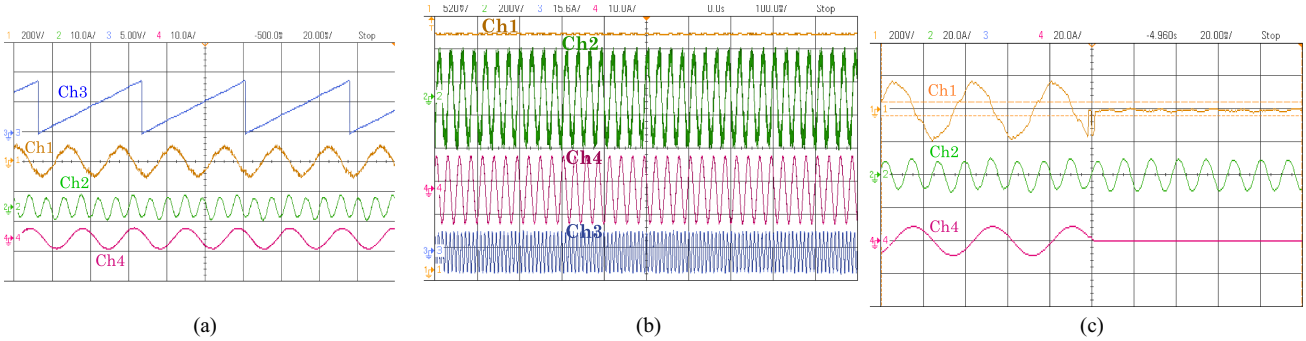

Fig. 31. Experimental Results. (a) Combined operation of the proposed multipole PMaSynRM, Ch1: 4-pole inverter voltage; Ch2: 12-pole current; Ch3: Rotor mechanical angle; Ch4: 4-pole current, at 800 rpm; (X-axis:- 20 ms/div; Y-axis:- Ch1: 200 V/div; Ch2: 10 A/div; Ch3: 3.59 rd/div; Ch4: 10 A/div). (b) Output torque during combined operation at base speed, Ch1: Output torque; Ch2: 4-pole VSI line voltage; Ch3: 12-pole current; Ch4: 4-pole current, at 1100 r/min; (X-axis:- 100 ms/div; Y-axis:- Ch1: 2.08 Nm/div; Ch2: 200 V/div; Ch3: 15.6 A/div; Ch4: 10 A/div). (c) Currents and voltages at change-over point Ch1: 4-pole inverter voltage; Ch2: 12-pole current; Ch4: 4-pole current, during change-over; (X-axis:- 20 ms/div; Y-axis:- Ch1: 200 V/div; Ch2: 20 A/div; Ch4: 20 A/div).

Here, it is observed from Ch. 1 that the back-EMF is negligible. Further, the current in Ch. 4 is zero, confirming no uncontrolled regeneration at high speeds. The torque at high speeds is also recorded and is presented in Fig. 33. From the scale of the Ch1 of the plot, the torque value can be calculated to be approximately 1 N · m.

2) Experimental Torque Speed and Efficiency Plots of the Proposed Machine: While the speed capability of the machine in combined mode is much higher and can theoretically extend to infinity, an early speed cut off can be performed based on the efficiency of the 4-pole winding, which deteriorates in the FW region. In the simulation, this cut-off speed is shown to be near 4000 r/min. However, the maximum speed of the loading motor of the experimental setup has to be restricted to 2400 r/min, which then becomes the maximum speed for 12-pole operation. Hence, to demonstrate a wide speed operation of the 12-pole winding, the change-over operation is performed near 1500 r/min, as can be observed in Fig. 34. This does not reduce the significance of the change-over results, as 1500 r/min corresponds to the FW region of the SynRM winding, and thus, the results validate the ease of the changeover process in the FW region. The back-EMF corresponding to the change-over

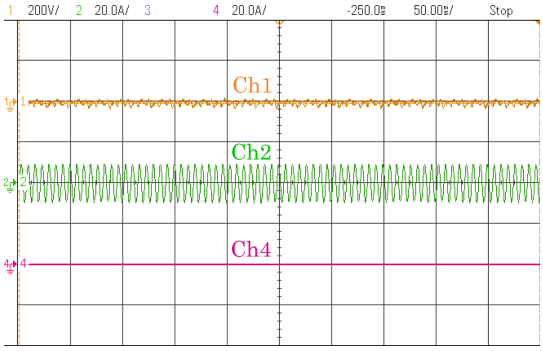

Fig. 32. Result showing negligible back-EMF in SynRM winding at 1500 r/min after change-over, Ch1: 4-pole back-EMF; Ch2: 12-pole current; Ch4: 4-pole current, after change-over; (X-axis:- 50 ms/div; Y-axis:- Ch1: 200 V/div; Ch2: 20 A/div; Ch4: 20 A/div).

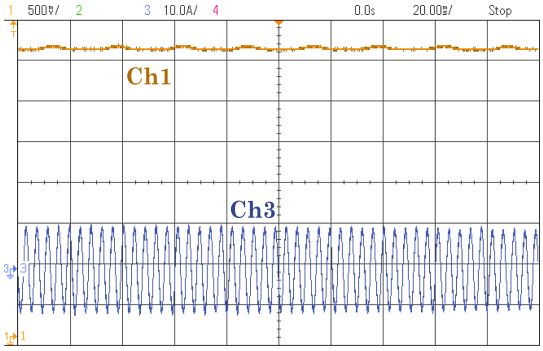

Fig. 33. Output torque during high speeds, Ch1: Output torque; Ch4: 12-pole current, at 2400 r/min; (X-axis:- 20 ms/div; Y-axis:- Ch1: 2.08 N · m/div; Ch4: 10 A/div).

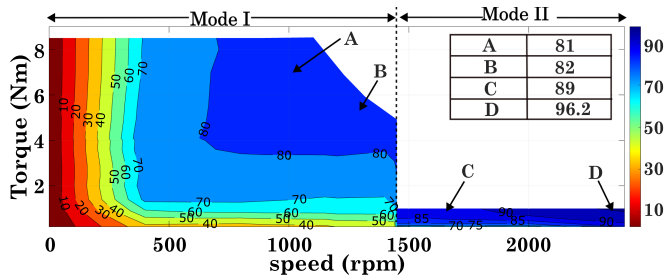

Fig. 34. Experimental torque-speed and efficiency plots.

speed has already been presented in Fig. 32. Another motivation for the changeover is the improvement in efficiency, which is demonstrated using the experimental efficiency plot presented in Fig. 34. The experimental efficiency is calculated using the ratio of the mechanical power output from the motor to the electrical power input to the motor measured at the terminals of the inverters. Since at higher speed ranges, only PM windings are excited, the effective resistance of the machine is reduced, thus reducing the copper losses. The efficiency also improves to 96.2%. Some of the data points are highlighted, and their corresponding efficiencies are also presented in Fig. 34.

V. Conclusion

In this article, a comprehensive analysis of the multipole permanent magnet-assisted synchronous reluctance machine, highlighting its unique design features and operational advantages, is presented. By carefully designing the stator and rotor to incorporate two distinct pole numbers, the machine delivers high output torque while maintaining efficiency over a wide speed range. Using independent windings for each pole minimizes interaction between them, enabling precise control of excitation and improving the performance and adaptability. Moreover, the back-EMF induced in the reluctance windings due to PM flux is negligible, making change-over operation possible without the need for mechanical switches, thereby simplifying operation and reducing maintenance requirements. In summary, the findings outlined in this study pave the way for the development of highly efficient and versatile electric machines for applications demanding high CPSR.

References

[1] R. Krishnan, "Introduction to permanent magnets and machines and converters and control," in *Permanent Magnet Synchronous and Brushless DC Motor Drives*. CRC press, 2010, ch. 1, pp. 3–134, doi: 10.1201/9781420014235.

[2] Y. Yang et al., "Design and comparison of interior permanent magnet motor topologies for traction applications," *IEEE Trans. Transp. Electrific.*, vol. 3, no. 1, pp. 86–97, Mar. 2017.

[3] B. B. St-Jacques, R. Shi, and P. Pillay, "An enhanced PMSM cooling design for traction of an electric vehicle," *IEEE Trans. Transp. Electrific.*, vol. 10, no. 2, pp. 3845–3854, Jun. 2024.

[4] S. V. Nair et al., "An unequal split dual three-phase PMSM with extended torque-speed characteristics for automotive application," *IEEE Trans. Power Electron.*, vol. 37, no. 10, pp. 12437–12449, Oct. 2022.

[5] S. V. Nair, "Design considerations for a symmetric dual three-phase IPMSM for battery electric vehicles," in *Proc. IEEE Int. Conf. Power Electron., Smart Grid, Renewable Energy*, 2022, pp. 1–7.

[6] M. Murataliyev, M. Degano, M. Di Nardo, N. Bianchi, and C. Gerada, "Synchronous reluctance machines: A comprehensive review and technology comparison," *Proc. IEEE*, vol. 110, no. 3, pp. 382–399, Mar. 2022.

[7] A. Vagati, G. Franceschini, I. Marongiu, and G. Troglia, "Design criteria of high performance synchronous reluctance motors," in *Proc. Conf. Rec. 1992 IEEE Ind. Appl. Soc. Annu. Meeting*, 1992, pp. 66–73.

[8] T. A. Lipo, "Synchronous reluctance machines-a viable alternative for ac drives?," *Electric Mach. Power Syst.*, vol. 19, no. 6, pp. 659–671, 1991.

[9] J.-R. Riba, C. López-Torres, L. Romeral, and A. Garcia, "Rare-earth-free propulsion motors for electric vehicles: A technology review," *Renewable Sustain. Energy Rev.*, vol. 57, pp. 367–379, 2016.

[10] Y. Xie et al., "Novel PM-assisted synchronous reluctance machines using asymmetrical rotor configuration," *IEEE Access*, vol. 10, pp. 79564–79573, 2022.

[11] E. Trancho et al., "PM-assisted synchronous reluctance machine flux weakening control for EV and HEV applications," *IEEE Trans. Ind. Electron.*, vol. 65, no. 4, pp. 2986–2995, Apr. 2018.

[12] S. V. Nair, P. Harikrishnan, and K. Hatua, "Six-step operation of a symmetric dual three-phase PMSM with minimal circulating currents for extended speed range in electric vehicles," *IEEE Trans. Ind. Electron.*, vol. 69, no. 8, pp. 7651–7662, Aug. 2021.

[13] A. Shah Mohammadi et al., "Hybridisation ratio for hybrid excitation synchronous motors in electric vehicles with enhanced performance," *IET Elect. Syst. Transp.*, vol. 8, no. 1, pp. 12–19, 2018.

[14] F. G. Capponi, G. Borocci, G. De Donato, and F. Caricchi, "Flux regulation strategies for hybrid excitation synchronous machines," *IEEE Trans. Ind. Appl.*, vol. 51, no. 5, pp. 3838–3847, Sep.–Oct. 2015.

[15] S. Atiq et al., "Wide speed range operation of non-salient PM machines," *IEEE Trans. Energy Convers.*, vol. 31, no. 3, pp. 1179–1191, Sep. 2016.

[16] J.-i. Itoh and K. Tanimukai, "Seamless star-delta winding changeover circuit for AC generators," in *Proc. Int. Conf. Renewable Energy Res. Appl.*, 2015, pp. 938–943.

[17] Y. Shin et al., "A thyristor-based seamless winding changeover circuit for high efficiency of electric vehicle drive system," in *Proc. 10th Int. Conf. Power Electron. ECCE Asia*, 2019, pp. 1274–1279.
[18] S.-H. Im and B.-G. Gu, "A snubberless solid-state tap changer for permanent magnet synchronous motors," *IEEE Trans. Power Electron.*, vol. 35, no. 11, pp. 12143–12152, Nov. 2020.
[19] K. Layek, S. V. Nair, and K. Hatua, "A tapped winding interior permanent magnet synchronous machine for medium-duty delivery trucks," *IEEE Trans. Transp. Electrific.*, vol. 10, no. 3, pp. 7420–7430, Sep. 2024.
[20] L. J. Hunt, "A new type of induction motor," *J. Inst. Elect. Eng.*, vol. 39, no. 186, pp. 648–667, 1907.
[21] A. Kusko et al., "Speed control of a single-frame cascade induction motor with slip-power pump back," *IEEE Trans. Ind. Appl.*, vol. IA-14, no. 2, pp. 97–105, Mar. 1978.
[22] Y. Gao, H. Maghbelli, M. Ehsani, G. Frazier, J. Kajs, and S. Bayne, "Investigation of proper motor drive characteristics for military vehicle propulsion," in *Proc. Future Transp. Technol. Conf. Expo.*, 2003, pp. 1–7, doi: 10.4271/2003-01-2296.
[23] D.-K. Ngo, M.-F. Hsieh, and T. A. Huynh, "Torque enhancement for a novel flux intensifying PMA-SYNRM using surface-inset permanent magnet," *IEEE Trans. Magn.*, vol. 55, no. 7, 2019, Art. no. 8106108.
[24] T. A. Huynh, M.-F. Hsieh, K.-J. Shih, and H.-F. Kuo, "An investigation into the effect of pm arrangements on PMA-SYNRM performance," *IEEE Trans. Ind. Appl.*, vol. 54, no. 6, pp. 5856–5868, Nov./Dec. 2018.
[25] A. Nagarkar and S. Srinivas, "An optimized rotor design of synchronous reluctance motor for improved torque characteristics," in *Proc. Int. Aegean Conf. Elect. Machines Power Electron./ Int. Conf. Optim. Elect. Electron. Equip.*, 2021, pp. 107–114.
[26] G. Choi and T. M. Jahns, "Analysis and design recommendations to mitigate demagnetization vulnerability in surface PM synchronous machines," *IEEE Trans. Ind. Appl.*, vol. 54, no. 2, pp. 1292–1301, Mar./Apr. 2018.
[27] A. Elhaj et al., "MTPA speed control for IPMSM drives without current sensing," *IEEE Access*, vol. 12, pp. 11411–11422, 2024.
[28] J. Pyrhonen, T. Jokinen, and V. Hrabovcova, "Design process of rotating electrical machines," in *Design of Rotating Electrical Machines*. Wiley, 2013, ch. 6, pp. 293–330, doi: 10.1002/9781118701591.ch6.
[29] T. A. Lipo, "Principles of design," in *Introduction to AC Machine Design*. Wiley, 2017, ch. 6, pp. 251–303, doi: 10.1002/9781119352181.ch6.
[30] W. L. Soong and T. Miller, "Field-weakening performance of brushless synchronous AC motor drives," *IEE Proc.-Electric Power Appl.*, vol. 141, no. 6, pp. 331–340, 1994.
[31] A. Vagati, M. Pastorelli, G. Francheschini, and S. Petrache, "Design of low-torque-ripple synchronous reluctance motors," *IEEE Trans. Ind. Appl.*, vol. 34, no. 4, pp. 758–765, Jul./Aug. 1998.
[32] Y. Wang et al., "Geometry analysis and optimization of PM-assisted reluctance motors," in *Proc. 22nd Int. Conf. Elect. Mach.*, 2016, pp. 1756–1762.
[33] A. Vagati, G. Franceschini, I. Marongiu, and G. Troglia, "Design criteria of high performance synchronous reluctance motors," in *Proc. Conf. Rec. IEEE Ind. Appl. Soc. Annu. Meeting*, 1992, pp. 66–73.
[34] E. C. Lovelace, T. M. Jahns, T. A. Keim, and J. H. Lang, "Mechanical design considerations for conventionally laminated, high-speed, interior PM synchronous machine rotors," *IEEE Trans. Ind. Appl.*, vol. 40, no. 3, pp. 806–812, May/Jun. 2004.
[35] ANSYS Inc., "Motor-CAD material library," Canonsburg, PA, USA, 2025. [Online]. Available: https://www.ansys.com/en-in/products/electronics/ansys-motor-cad

Veena Prasanna (Student Member, IEEE) was born in Kerala, India. She received the B.Tech degree in electrical engineering from Jyoti Engineering College, Kerala, India, in 2018. She is currently working toward an integrated M.S. and Ph.D. from the Electrical Engineering Department, Indian Institute of Technology Madras, Chennai, India.

Her research interests include design of permanent magnet synchronous machines, synchronous reluctance machines and multipole permanent magnet-assisted synchronous reluctance machines for EV applications.

Kunal Layek (Member, IEEE) was born in Durgapur, West Bengal, India. He received the B.Tech. degree in electrical engineering from Asansol Engineering College, Asansol, India, in 2013. He received an integrated M.S. and Ph.D. from IIT Madras, Chennai, India, in 2025.

He is currently working as a Postdoctoral Researcher with the Department of Electrical and Computer Engineering, University of Illinois at Urbana-Champaign, USA. His research interests include PMSM drives for EV and wind turbine applications.

Kamalesh Hatua (Member, IEEE) was born in West Bengal, India. He received the Ph.D. degree in electrical engineering from the IISC Bangalore, Karnataka, India, in 2011.

He was with BEM Ltd., Mysore, India, and Honeywell Technology Solutions Laboratory, Bangalore, India. He was a Postdoctoral Research Fellow with the FREEDM Center, NCSU, Raleigh, NC, USA. He is currently an Associate Professor with the Department of EE, IIT Madras, India. His research interests include medium-voltage electric drives, automotive drives, polyphase induction motor drives, active gate driving for SiC switches, solid-state transformer, and design of highly efficient power converters using SiC power switches.